

Simulation of an Irregular Free Surface with a Displacement Finite-Difference Scheme

by J. A. Pérez-Ruiz, F. Luzón, and A. García-Jerez

Abstract In this article, we present a method to simulate wave propagation in a 2D medium with an irregular free surface by using a finite-difference method. The free-surface conditions are developed through an explicit scheme in displacement. In our technique, a conventional grid is used to define the zone where there is material and the zone where there is not material. In this method a fictitious line of material above the free surface is used to compute the displacement at the free surface. A classification of the points that shape the fictitious line is presented. Then displacements in the internal points of the material are computed together with the displacements at the points of the free surface, and subsequently the displacement at the points of the fictitious line are updated applying the boundary conditions by using an explicit finite-difference scheme. We present some results of the application of this technique by means of the simulation of the seismic response of a canyon and a mountain using an explosive source and a vertical force, respectively. We compared the results with the synthetics calculated by the indirect boundary element method (IBEM). First, we tested the method simulating the wave propagation at a half-space with a planar surface. The comparison with the results of the IBEM gave us confidence to deal with other models with topography features. These topographical models provided results that were in very good agreement with the results obtained by the IBEM.

Introduction

Irregular topography can affect earthquake displacement (Bard, 1994; Sánchez-Sesma, 1996). Spatial variability of amplification can be observed together with characteristic polarization patterns. The simulation of this kind of effect at irregular topographies and its understanding is therefore of interest for seismology. This problem is taken into account using the traction-free boundary conditions, but this task has an inherent difficulty when techniques such as the finite-difference method are used, (Moczo *et al.*, 2004).

The use of techniques such as the boundary element (Sánchez-Sesma and Luzón, 1995) or the discrete wavenumber method (Aki and Larner, 1970) have been popular for relatively simple geometry and geological conditions. On the other hand, finite-element (Bielack *et al.*, 2003) and finite-difference (Alterman and Karal, 1968; Graves, 1996) methods are better suited for more realistic models with highly heterogeneous materials. Alterman and Karal (1968) solved the problem of a layer on a half-space directly with the equations of the boundary conditions (both stresses and displacements must be continuous at the interface, and stresses must vanish on the free surface). These conditions generated an implicit scheme. They used a nonstaggered displacement scheme and developed their algorithm for homogeneous me-

dia. Boore (1972) and Kelly *et al.* (1976) improved the algorithm for heterogeneous media. Boore introduced the so-called vacuum formalism for the 2D *SH* problem, in which the Lamé parameters and density are set to zero to simulate the free-surface boundary.

Munasinghe and Farnell (1973) solved the problem of Rayleigh wave scattering at vertical discontinuities. They used an extra line of points called pseudonodes to compute the behavior of the free surface. Kelly *et al.* (1976) introduced the arithmetic averages of the parameters in the scheme; this was called “heterogeneous formulation.” Furthermore these authors used a fictitious line above the free surface to compute the displacement at the horizontal free surface. Fuyuki and Matsumoto (1980) solved the problem of Rayleigh wave scattering at a trench; they used an extra line of pseudonodes although with a procedure different from the one followed by Munasinghe and Farnell (1973). Ilan (1977) and Rong-Song *et al.* (1988) used the finite-difference (FD) method to simulate *P-SV* wave propagation in an elastic medium with a polygonal free surface. These schemes required a nonuniform grid, introducing some complexity and decreasing the accuracy. Levander (1988) developed the stress-imaging technique, in which it was nec-

essary to know the values of the stress-tensor components above the free surface. He developed a velocity-stress, staggered-grid scheme with a fourth order approximation. Sochacki *et al.* (1991) performed a modification of the heterogeneous formulation of Kelly *et al.* (1976), introducing some differences in his finite-difference schemes because they explicitly accounted for the boundary conditions and more emphasis was placed on the time derivative. Zahradnik *et al.* (1994), in contrast to Sochacki, integrated the rigidity parameter and made use of the weighted arithmetic averages to deal the interface boundary condition. They introduced, the vacuum formalism for 2D P - SV problem, where the parameters above the free surface are placed to zero, and the same scheme of the internal points of model was used to compute the displacements at the free surface. Zahradnik and Priolo (1995) presented an important work in which they justified the heterogeneous formulation of Boore (1972) and Kelly *et al.* (1976). They used the vacuum formalism to deal with the free surface and gave a theoretical justification using the arithmetic averages to reproduce the behavior of the interface boundary conditions. Later, Graves (1996) employed the same stress-imaging technique as Levander (1988), with a 3D problem. Graves used the stress-imaging technique as a zero-stress formulation and compared it with the vacuum formulation. He observed that the zero-stress formulation obtained better results when compared to the frequency-wavenumber technique. Ohminato and Chouet (1997) discretized the 3D topography in a staircase by stacking unit material cells in a staggered-grid scheme. The shear stresses are distributed on the 12 edges of the unit material cell so that only shear stresses appear on the free surface and normal stresses always remain embedded within the solid region. Oprsal and Zahradnik (1999) introduced a new scheme that uses irregular grids to solve the problem of wave propagation. They used geometric averages to weight the parameters of the medium and when the interface between two different media did not agree with a grid point's line. Hayashi *et al.* (2001) used a mixed technique that combined the generalized image method and the vacuum formalism in a viscoelastic velocity-stress, staggered-grid scheme. This technique had two problems, the proposed free-surface condition required at least 30 grid points per wavelength, and the discontinuous grid computation was eventually unstable. Ruud and Hestholm (2001) used a curved grid in the (x, z) system to model the topography, changing the system of coordinates with a displacement-stress scheme. Kristek *et al.* (2002) used a different technique based on the adjusted FD approximations (AFDA). This technique is different from the stress-imaging technique, and no virtual-displacement/particle-velocity and stress-tensor values above the free surface were used. Moczo *et al.* (2004) used this technique to calculate ground motion in models with lateral material discontinuities and planar free surface. Both, Kristek *et al.* (2002) and Moczo *et al.* (2004), used fourth-order staggered-grid, stress-velocity FD schemes. Finally, Min *et al.* (2004) worked in the frequency domain with a displacement scheme

and proposed the use of a cell-based grid set where material properties are defined within cells rather than at nodal points. The properties in cells are calculated by arithmetic averages of adjacent points, and the free surface is computed assuming that material properties above the free surface are zero.

This article presents a method to compute the displacement at a free surface with irregular geometry. This is a simple implementation of stress-free boundary conditions for topographies of arbitrary shape with a 2D displacement FD scheme. Our method is flexible and allows the study of complex topographies. We tested the validity of this method by comparing our results with those computed with the indirect boundary element method (IBEM) (Sánchez-Sesma and Campillo, 1993).

Equations of Motion and Free-Surface Conditions

In our scheme x and z are the horizontal and vertical rectangular coordinates in a 2D medium. The z axis is positive downward, and the x axis is positive to the right. Two coupled, second-order, partial differential equations can be used to describe the motion of P waves and vertically polarized shear SV waves in a medium. These two equations of motion are

$$\rho \left(\frac{\partial^2 u}{\partial t^2} \right) = (\lambda + 2\mu) \left(\frac{\partial^2 u}{\partial x^2} \right) + \mu \left(\frac{\partial^2 u}{\partial z^2} \right) + \lambda \left(\frac{\partial^2 w}{\partial x \partial z} \right) + \mu \left(\frac{\partial^2 w}{\partial z \partial z} \right) \quad (1)$$

$$\rho \left(\frac{\partial^2 w}{\partial t^2} \right) = \mu \left(\frac{\partial^2 w}{\partial x^2} \right) + (\lambda + 2\mu) \left(\frac{\partial^2 w}{\partial z^2} \right) + \mu \left(\frac{\partial^2 u}{\partial x \partial z} \right) + \lambda \left(\frac{\partial^2 u}{\partial z \partial z} \right) \quad (2)$$

where ρ is the density, u and w are the horizontal and vertical displacement, respectively, λ and μ are the Lamé parameters, and t is time.

We use a regular, rectangular grid with steps Δx and Δz . Following the diagram of Figure 1, we give some examples of the FD approximations for nonmixed (equation 3) and mixed (equation 6) derivatives (Pérez-Ruiz and Luzón, 2004). Here the subscripts i, j correspond to the spatial position (j to x and i to z), and subscript k gives the time step,

$$\frac{\partial}{\partial x} \left(p \frac{\partial f}{\partial x} \right)_{i,j} = 2 \frac{1}{\Delta x(j-1) + \Delta x(j)} \left(p_r \frac{f(i, j+1, k) - f(i, j, k)}{\Delta x(j)} - p_l \frac{f(i, j, k) - f(i, j-1, k)}{\Delta x(j-1)} \right) \quad (3)$$

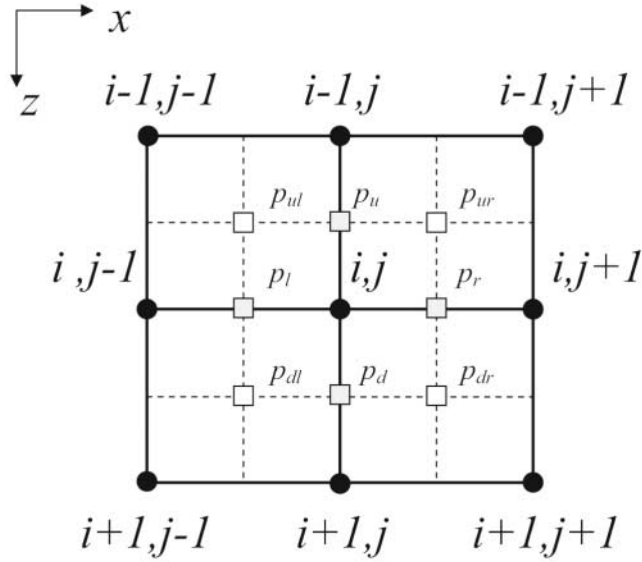


Figure 1. Example of FD grids cell with positions of the wave-field displacement and effective media parameters. In this figure the criterion followed by subscripts is observed. The media parameters are computed as the value of the geometric average of adjacent points of the grid.

with

$$p_r = \sqrt{p(i, j + 1) \cdot p(i, j)} \quad (4)$$

$$p_l = \sqrt{p(i, j) \cdot p(i, j - 1)} \quad (5)$$

and mixed derivative,

$$\frac{\partial}{\partial z} \left(p \frac{\partial f}{\partial x} \right)_{i,j} = \frac{1}{2} \frac{1}{\Delta z(i - 1) + \Delta z(i)}.$$

$$\left(\begin{array}{l} p_{dr} \frac{1}{\Delta x(j)} (f(i, j + 1, k) + f(i + 1, j + 1, k) - f(i, j, k) - f(i + 1, j, k)) + \\ + p_{dl} \frac{1}{\Delta x(j - 1)} (f(i, j, k) + f(i + 1, j, k) - f(i, j - 1, k) - f(i + 1, j - 1, k)) - \\ - p_{ur} \frac{1}{\Delta x(j)} (f(i - 1, j + 1, k) + f(i, j + 1, k) - f(i - 1, j, k) - f(i, j, k)) - \\ - p_{ul} \frac{1}{\Delta x(j - 1)} (f(i - 1, j, k) + f(i, j, k) - f(i - 1, j - 1, k) - f(i, j - 1, k)) \end{array} \right) \quad (6)$$

with

$$p_{dr} = \sqrt[4]{p(i, j + 1) \cdot p(i + 1, j + 1) \cdot p(i, j) \cdot p(i + 1, j)} \quad (7)$$

$$p_{dl} = \sqrt[4]{p(i, j) \cdot p(i + 1, j) \cdot p(i, j - 1) \cdot p(i + 1, j - 1)} \quad (8)$$

$$p_{ur} = \sqrt[4]{p(i - 1, j + 1) \cdot p(i, j + 1) \cdot p(i - 1, j) \cdot p(i, j)} \quad (9)$$

$$p_{ul} = \sqrt[4]{p(i - 1, j) \cdot p(i, j) \cdot p(i - 1, j - 1) \cdot p(i, j - 1)} \quad (10)$$

where p is an elastic parameter of the medium and f is the vertical or horizontal component of the displacement. The subscripts of parameter p refer to down (d), up (u), left (l), and right (r); they indicate the movement over the grid around the (i, j) -point (see Fig. 1). In this respect, we use the idea of Min *et al.* (2004). We use a cell-based grid but apply the free-surface condition directly. We use geometric averages for the elastic parameters of the medium. This allows computing correct values of the displacement on the interface between two different media; it is not necessary to employ the continuity boundary conditions directly.

Also the stability of our FD approximation requires the following condition (Marfurt, 1984);

$$\Delta t < \frac{h}{\sqrt{\alpha^2 + \beta^2}}, \quad (11)$$

where h is the step of the grid, Δt is the time step, and α and β are the maximum velocities of P and S waves in the media. The nondispersion criterion used is given by

$$h_{\min} = \frac{\beta_{\min}}{10 \cdot f_{\max}}, \quad (12)$$

where β_{\min} is the minimum velocity of S waves and f_{\max} defines the limit of the range of frequencies that can be simulated in the model. If the source is modeled by a Ricker wavelet this frequency can be calculated as three times the frequency of the pulse. As shown by Moczo *et al.* (2000), a minimum of 10 points per wavelength are necessary to minimize the effects of grid dispersion and to achieve good accuracy.

The most obvious way to implement a free-surface condition is to constrain the solution by applying equations directly at the free surface. The vanishing of normal tractions on the free-surface boundary is imposed by the equation $T_j(\vec{u}, \vec{n}) = \sigma_{ij}n_i = 0$ at the free surface $z = 0$, with n unit vector normal to the surface. In this problem four general cases have been considered:

1. Horizontal free surface:

$$\sigma_{zz} = \lambda \frac{\partial u}{\partial x} + (\lambda + 2\mu) \frac{\partial w}{\partial z} = 0 \quad (13)$$

$$\sigma_{zx} = \mu \frac{\partial w}{\partial x} + \mu \frac{\partial u}{\partial z} = 0 \quad (14)$$

2. Vertical free surface:

$$\sigma_{xx} = (\lambda + 2\mu) \frac{\partial u}{\partial x} + \lambda \frac{\partial w}{\partial z} = 0 \quad (15)$$

$$\sigma_{xz} = \mu \frac{\partial u}{\partial z} + \mu \frac{\partial w}{\partial x} = 0 \quad (16)$$

3. Exterior corner of free surface:

$$\begin{aligned} \sigma_{xx} - \sigma_{xz} &= (\lambda + 2\mu) \frac{\partial u}{\partial x} \\ &+ \lambda \frac{\partial w}{\partial z} - \mu \frac{\partial u}{\partial z} - \mu \frac{\partial w}{\partial x} = 0 \end{aligned} \quad (17)$$

$$\begin{aligned} -\sigma_{zz} + \sigma_{zx} &= -\lambda \frac{\partial u}{\partial x} - (\lambda + 2\mu) \frac{\partial w}{\partial z} \\ &+ \mu \frac{\partial w}{\partial x} + \mu \frac{\partial u}{\partial z} = 0 \end{aligned} \quad (18)$$

4. Interior corner of free surface:

$$\begin{aligned} \sigma_{xx} - \sigma_{xz} &= (\lambda + 2\mu) \frac{\partial u}{\partial x} \\ &+ \lambda \frac{\partial w}{\partial z} - \mu \frac{\partial u}{\partial z} - \mu \frac{\partial w}{\partial x} = 0 \end{aligned} \quad (19)$$

$$\begin{aligned} -\sigma_{zz} + \sigma_{zx} &= -\lambda \frac{\partial u}{\partial x} - (\lambda + 2\mu) \\ &\frac{\partial w}{\partial z} + \mu \frac{\partial w}{\partial x} + \mu \frac{\partial u}{\partial z} = 0 \end{aligned} \quad (20)$$

These are the general equations that govern the behavior of free surface, which have to be approximated using finite differences. These expressions are approximated by diverse FD schemes according to the kind of point on the free surface.

We have checked that the geometric average provides a better behavior than the arithmetic average in terms of major stability and convergence. When the model is heterogeneous we achieve long times with a very stable behavior of the scheme. This scheme is conditionally stable according to equation (11), but to solve the free-surface problem it is necessary to combine two different schemes: the general scheme for the internal points and the specific scheme for the points at the fictitious line. This stress condition for the horizontal free surface is divided in two conditions, the tangential and the normal stresses. Kelly *et al.* (1976) employed zero-stress condition too, but in the tangential stress condition (equation 14) they simplified the rigidity modulus μ leaving only the spatial derivatives. Following these authors, we made some computations using arithmetic averages in the general scheme and in the parameters that appear at the normal stress condition (equation 13). We observed that the method was stable but its results and those obtained with the IBEM were not in good agreement. It was logical to think that if arithmetic averages were employed in the elastic parameters of both conditions (equations 13 and 14) the method could be still more accurate. With this idea some tests with heterogeneous basins were realized and the scheme became unstable. At last, following the idea of Oprsal and Zahradnik (1999), we achieved the stability and convergence of the method using geometric averages at the schemes for the internal points and for the points of the fictitious line.

Implementation

To implement our FD scheme to an arbitrary topography, we first define a matrix with ones [1], zeros [0] and the nonreflecting boundaries [B] as shown in Figure 2. In this matrix the ones represent the material, whereas the zeros represent the zone where there is no material.

In our scheme we use fictitious material on the line above the free surface. The grid line above the free surface is necessary because of the expansion by FD of equations (13) to (20). To apply the free-boundary conditions it is necessary to define 12 types of points on the fictitious line. We classified these points as shown in Table 1. The number that identified each kind of point of the fictitious line indicates the order of update. Various examples are shown in Figure 3a and b. Although the boundary condition is the same on the entire free surface, each kind of point requires a different equation to be used.

To deal with an explicit FD scheme, the computation has to be carried out in a specific order. First the interior points [1] are computed with the approximation by finite differences of equations (1) and (2). Then the interior corners

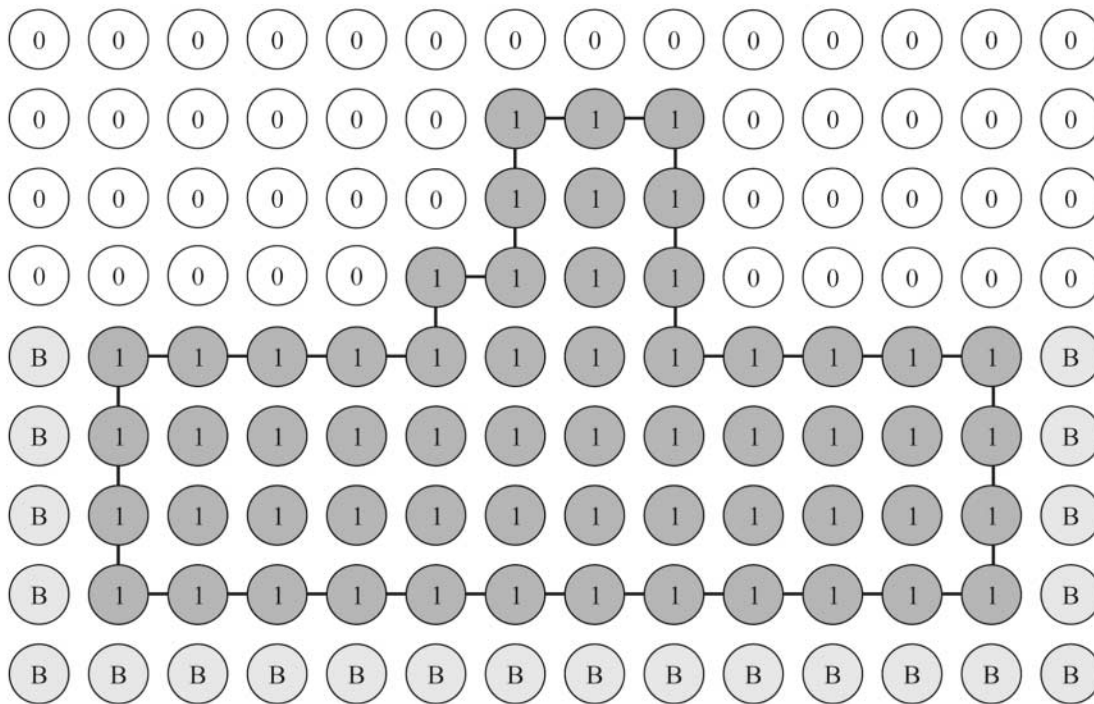


Figure 2. Matrix with ones and zeros that define the model. In this matrix only, there are ones, zeros, and the points of nonreflecting boundaries (B).

of the fictitious line [2], [3], [4], and [5] are computed, after that the horizontal and vertical points of fictitious line [6], [7], [8], and [9], and then the exterior corners [10], [11], [12], and [13]. Finally, the nonreflecting boundaries are computed. In this way the displacements at the free surface can be obtained at the next time step. This procedure is comparable to those followed by Kelly *et al.* (1976), Munasinghe and Farnell (1973), and Fuyuki and Matsumoto (1980). The principal difference from these works is that the method here presented is a general procedure to solve free surfaces with arbitrary forms. In the work of Kelly *et al.* (1976), only horizontal free surface was treated (points labeled as [6] here) using the fictitious line concept. An important difference between our work and the works of Munasinghe and Farnell (1973) and Fuyuki and Matsumoto (1980), who used the pseudonode concept introduced by Peaceman (1966), is in the process of computing the corners. In our treatment, the displacements at all the points of the fictitious line, including the corners, are computed by their corresponding scheme, and all internal points labeled as [1] are calculated by a same general numerical scheme, including the displacements at the free surface. Nevertheless, in the method by Fuyuki and Matsumoto (1980) the displacements at those pseudonodes that were equivalent to the exterior corners of our fictitious line were not computed. Therefore different schemes were used to update the displacements at some internal points of the model; for example, the exterior corners of the free surface. Equally, the displacements at the pseudonodes that were equivalent to the interior corners of our fic-

titious line were not calculated either and two new intermediate pseudonodes at the grid were necessary to compute the adjacent internal points, which were updated with specific numerical schemes. Their procedure was similar to that developed by Munasinghe and Farnell (1973) although with some slight differences with regard to the schemes used. In these works, the points labeled here as [4], [5], [7], [12], and [13] were not treated. These points allow us to study cavities as shown in Figure 3b.

Along the fictitious line the media parameters have the same values as in the medium. This fact is easy to understand for points [6], [7], [8], and [9] on the horizontal and vertical fictitious line, likewise for the exterior corners. However, when the union of two different materials is just placed in the adjacent points of an interior corner (see Fig. 4a) a reasonable doubt could appear about which material value might be used. As it is shown later any of both material values could be used. To study this particular situation, an example of this problem is presented. In Figure 4a, a model with two materials joined, forming a corner, is shown. Material A has an S -wave velocity $\beta_A = 1100$ m/sec and a P -wave velocity $\alpha_A = 2000$ m/sec. Material B has a S wave velocity $\beta_B = 570$ m/sec and a P -wave velocity $\alpha_B = 1000$ m/sec. Both materials have a density $\rho = 2000$ kg/m³. Three receivers are placed on the free surface of this model. A receiver is just situated on the interior corner, and the other receivers are placed above the vertical and horizontal free surface with a distance of 200 m from the interior corner. This model is excited by an explosive source. The time sig-

Table 1
Classification of the Points of the Fictitious Line and Their Stress Conditions

KIND OF FREE SURFACE	DETAIL	STRESS EQUATION	NUMBER POINT
<i>interior corner of free surface with material underneath and to the right:</i>		$-\sigma_{xx} - \sigma_{xz} = 0$ $-\sigma_{zz} - \sigma_{zx} = 0$	[2]
<i>interior corner of free surface with material underneath and to the left:</i>		$\sigma_{xx} - \sigma_{xz} = 0$ $-\sigma_{zz} + \sigma_{zx} = 0$	[3]
<i>interior corner of free surface with material above and to the right:</i>		$-\sigma_{xx} + \sigma_{xz} = 0$ $\sigma_{zz} - \sigma_{zx} = 0$	[4]
<i>interior corner of free surface with material above and to the left:</i>		$\sigma_{xx} + \sigma_{xz} = 0$ $\sigma_{zz} + \sigma_{zx} = 0$	[5]
<i>Horizontal free surface with material underneath:</i>		$\sigma_{zz} = \sigma_{zx} = 0$	[6]
<i>Horizontal free surface with material above:</i>		$-\sigma_{zz} = \sigma_{zx} = 0$	[7]
<i>Vertical free surface with material to the right:</i>		$-\sigma_{xx} = \sigma_{xz} = 0$	[8]
<i>Vertical free surface with material to the left:</i>		$\sigma_{xx} = \sigma_{xz} = 0$	[9]
<i>Exterior corner of free surface with material underneath and to the right:</i>		$-\sigma_{xx} - \sigma_{xz} = 0$ $-\sigma_{zz} - \sigma_{zx} = 0$	[10]
<i>Exterior corner of free surface with material underneath and to the left:</i>		$\sigma_{xx} - \sigma_{xz} = 0$ $-\sigma_{zz} + \sigma_{zx} = 0$	[11]
<i>Exterior corner of free surface with material above and to the right:</i>		$-\sigma_{xx} + \sigma_{xz} = 0$ $\sigma_{zz} - \sigma_{zx} = 0$	[12]
<i>Exterior corner of free surface with material above and to the left:</i>		$\sigma_{xx} + \sigma_{xz} = 0$ $\sigma_{zz} + \sigma_{zx} = 0$	[13]

nal is a Ricker wavelet with $t_p = 0.75$ sec, and $t_s = 1$ sec. This source is located 2 km toward the right and 1 km downward with regard to the interior corner. A time step $\Delta t = 0.006$ sec and a grid spacing $\Delta x = \Delta z = 20$ m were used. In Figure 4b, the synthetics recorded in the three receivers are presented. In this figure three results are shown: the solid line depicts the results using the fictitious line A, where the internal corner has the values of the material A; the crosses represent the results with the fictitious line B, where the interior corner has the values of the material B; and finally, the asterisks depict the solution considering the vacuum for-

malism in a FD scheme. The three results are in good agreement. This fact indicates that the values attributed to the interior corner do not concern the final result significantly. The reason for this agreement can owe to the employment of a cell-based grid scheme and the use of geometric averages.

As is shown in Table 1, each point of the free surface has to satisfy a particular condition with the appropriate components of stress. For example in the horizontal free surface with material underneath, the type of point labeled as [6], we can proceed in the following way:

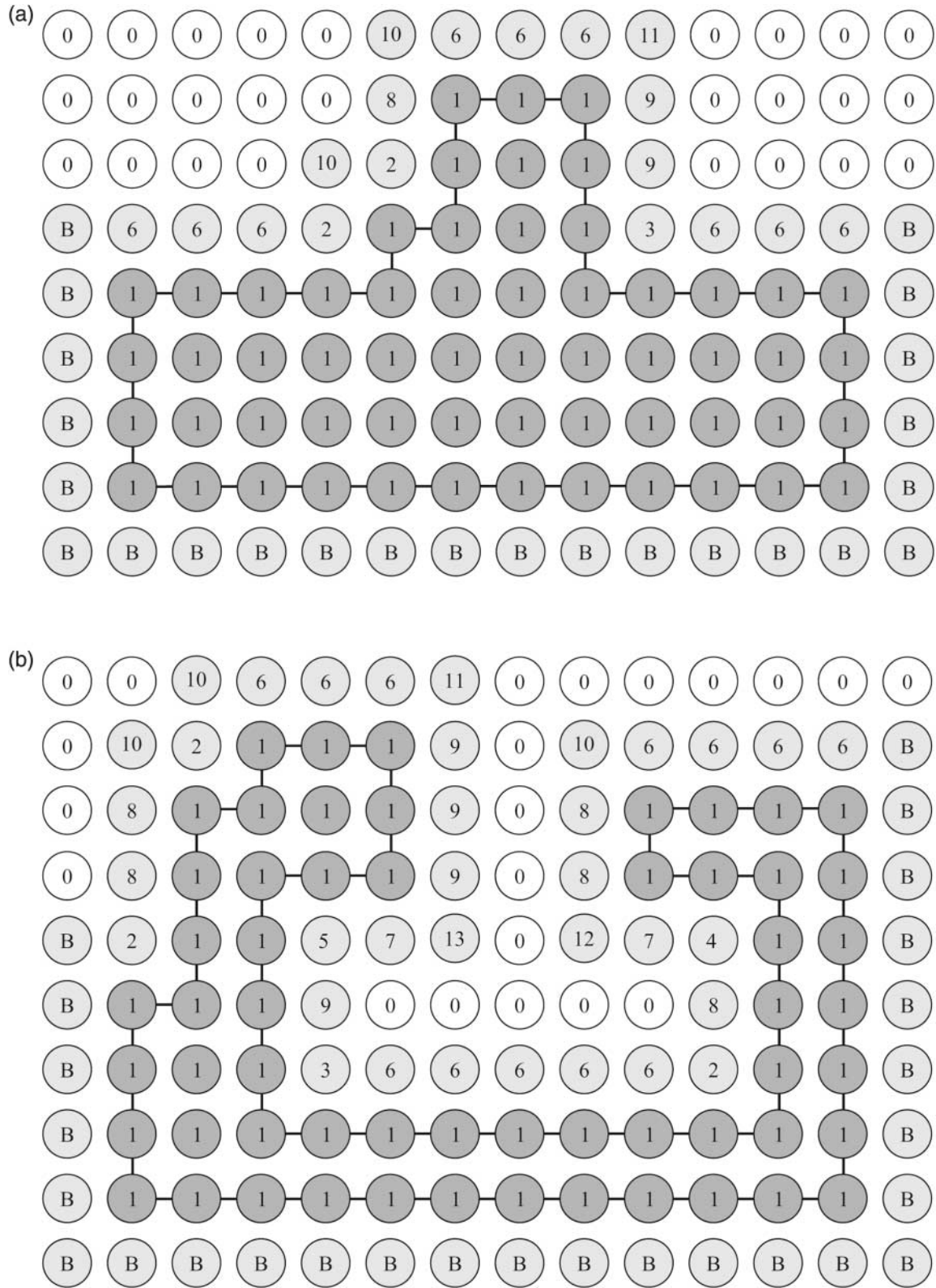


Figure 3. Matrixes where the classification of different points is observed. The points of this matrix are classified according to the shape of one free surface and we introduce the fictitious line above the real free surface. The interior points are labeled as 1 and nonreflecting boundaries are labeled as B. (a) The topography of an arbitrary mountain. (b) The topography of a cavity.

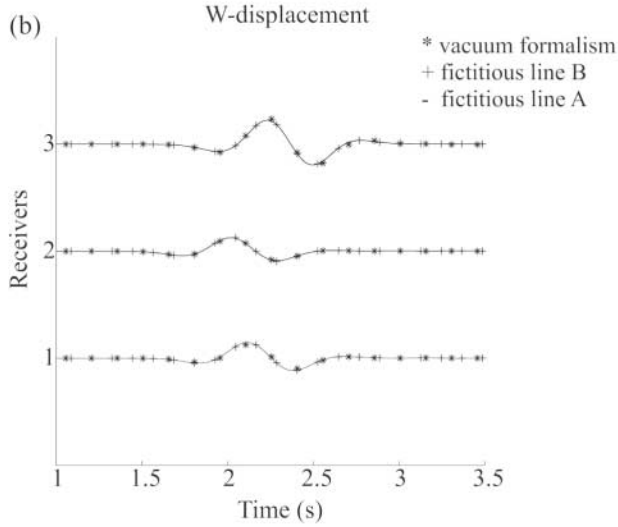
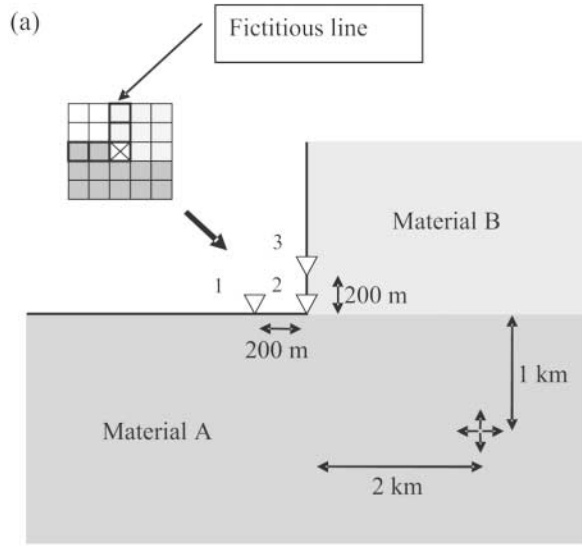


Figure 4. (a) Model to study the effect of an internal corner. The union of the two materials agrees with the internal corner. Three receivers are placed above the free surface. A detail of the fictitious line is shown. The crossed out cell depicts the internal corner at the fictitious line. This cell can support the values of material A or material B. This source is located 2 km toward the right and 1 km downward regarding the internal corner. (b) Vertical displacements W recorded in the three receivers. The solid line depicts the solution with fictitious line A, the pluses with the fictitious line B, and the asterisks with the vacuum formalism. The time signal is a Ricker wavelet with $t_p = 0.75$ sec and $t_s = 1$ sec.

$$\sigma_{zz} = \sigma_{zx} = 0 \quad (21)$$

$$\sigma_{zz} = \lambda \frac{\partial u}{\partial x} + (\lambda + 2\mu) \frac{\partial w}{\partial z} = 0 \quad (22)$$

$$\sigma_{zx} = \mu \frac{\partial w}{\partial x} + \mu \frac{\partial u}{\partial z} = 0 \quad (23)$$

Developing these equations by FD schemes we get,

$$\lambda_{cx} \left(\frac{u(i, j+1, k) - u(i, j-1, k)}{2\Delta x} \right) + (\lambda + 2\mu)_{cz} \left(\frac{w(i, j, k) - w(i-1, j, k)}{\Delta z} \right) = 0 \quad (24)$$

$$\mu_{cx} \left(\frac{w(i, j+1, k) - w(i, j-1, k)}{2\Delta x} \right) + \mu_{cz} \left(\frac{u(i, j, k) - u(i-1, j, k)}{\Delta z} \right) = 0 \quad (25)$$

and working out the value of the displacements at the point $(i-l, j, k)$, the final equations for a horizontal free surface with material underneath are:

$$w(i-1, j, k) = w(i, j, k) + \left(\frac{\Delta z}{2\Delta x} \right) \left(\frac{\lambda_{xc}}{(\lambda + 2\mu)_{cz}} \right) (u(i, j+1, k) - u(i, j-1, k)) \quad (26)$$

$$u(i-1, j, k) = u(i, j, k) + \left(\frac{\Delta z}{2\Delta x} \right) \left(\frac{\mu_{xc}}{\mu_{cz}} \right) (w(i, j+1, k) - w(i, j-1, k)) \quad (27)$$

where the Lamé parameters are defined as:

$$\lambda_{cx}(i, j) = \sqrt{\lambda(i, j+1) \cdot \lambda(i, j-1)} \quad (28)$$

$$(\lambda + 2\mu)_{cx}(i, j) = \sqrt{(\lambda + 2\mu)(i, j) \cdot (\lambda + 2\mu)(i-1, j)} \quad (29)$$

$$\mu_{cx}(i, j) = \sqrt{\mu(i, j+1) \cdot \mu(i, j-1)} \quad (30)$$

$$\mu_{cz}(i, j) = \sqrt{\mu(i, j) \cdot \mu(i-1, j)} \quad (31)$$

From equation (26) we can calculate $w(i-l, j, k)$, and from equation (27) we can compute $u(i-l, j, k)$ (see Fig. 5). These are the displacements on the fictitious line, that will be used to compute the displacements on the free surface with the approximation by FD of equations (1) and (2); this is the approximation for interior points of the model. Following this procedure we can get the formula of displacement at each kind of point of the fictitious line.

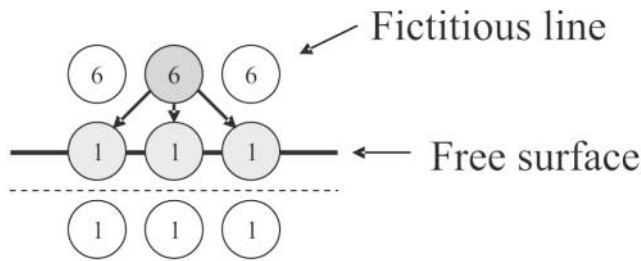


Figure 5. The point 6 of the fictitious line requires the three indicated points 1 to be actualized. Later, it will be possible to compute the displacements in the dark-gray point 1 of the free surface with displacements at points of the fictitious line, and internal points 1.

It is attractive to use a scheme that is totally explicit. This would avoid solving equation systems, and the procedure would be totally iterative, but there are some cases in which the discretization could introduce an implicit scheme, because of the order with which computations should be made. For example, when the internal points [1] and the entire interior corner are updated we might choose from two cases, to compute the displacement at the points [6] of the horizontal fictitious line first, or to compute the displacements at the points [8] of the vertical fictitious line first. If the points [6] are computed first, when this point [6] is an extreme left point equations (26) and (27) require the dis-

placements at a point [8] as seen in Figure 6a. Whereas if the extreme top point [8] is computed first its equation will need the adjacent point [6] (see Fig. 6b). That is, displacements are always needed at a point that has not been updated. Following with this example, we can observe that the displacements in the equations of a point [10]

$$u(i, j, k) = \left(\frac{\mu(i, j)}{2(\lambda + 2\mu)(i, j)} \right) (u(i + 1, j, k) + u(i, j + 1, k) - w(i + 1, j, k) + w(i, j + 1, k)) + \left(\frac{\lambda(i, j) + \mu(i, j)}{(\lambda + 2\mu)(i, j)} \right) u(i, j + 1, k) \quad (32)$$

$$w(i, j, k) = \left(\frac{\mu(i, j)}{2(\lambda + 2\mu)(i, j)} \right) (w(i + 1, j, k) - w(i, j + 1, k) + u(i + 1, j, k) + u(i, j + 1, k)) + \left(\frac{\lambda(i, j) + \mu(i, j)}{(\lambda + 2\mu)(i, j)} \right) w(i, j + 1, k), \quad (33)$$

require the displacements of the points [6] and [8] (see Fig. 6c). To solve this problem one can concentrate on the extreme point [6]. In this example we give attention to the

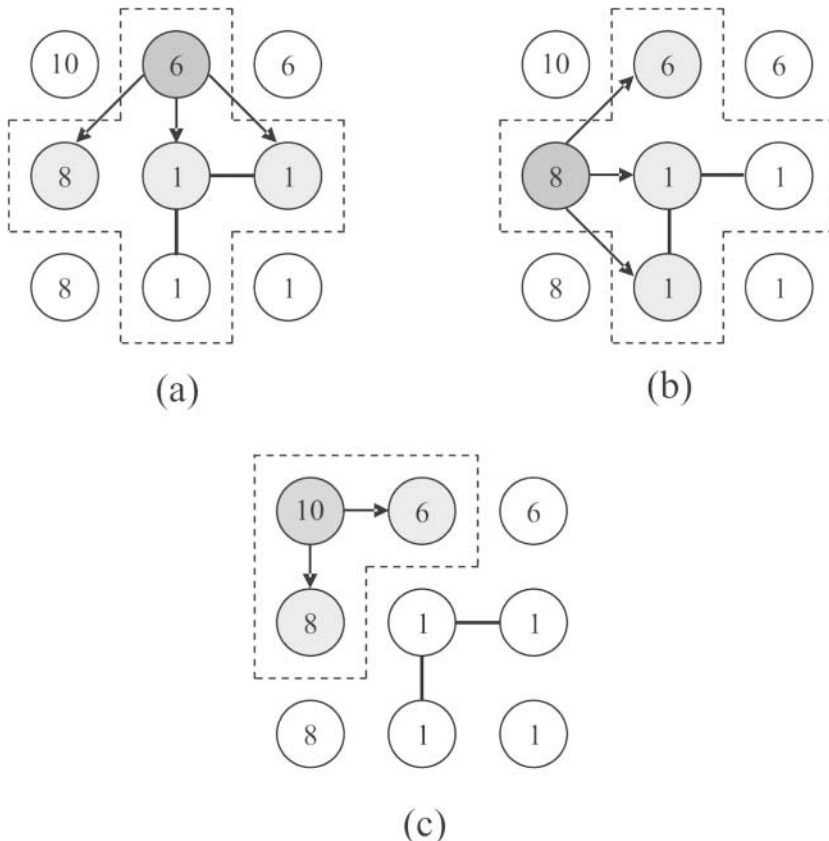


Figure 6. (a) Scheme to compute the displacement at the point 6 of the horizontal fictitious line; we can see that the displacement at the indicated adjacent point 8 still is not updated. (b) Scheme to compute the displacement at the point 8 of the vertical fictitious line; we can see that the displacement at the indicated adjacent point 6 still is not updated. (c) Scheme to compute the displacements at the point 10, it is necessary to know the displacements in adjacent points 6 and 8, but these displacements still have not been updated.

left extreme point [6], and other FD schemes can be used to approximate the displacement at this point. Instead of using a centered FD scheme to approximate the horizontal derivative, it is possible to use a forward FD scheme at this point, as follows:

$$w(i-1, j, k) = w(i+1, j, k) + \left(\frac{2\Delta z}{12\Delta x}\right) \left(\frac{\lambda_{cx}}{(\lambda + 2\mu)_{cz}}\right) (-u(i, j+2, k) + 4u(i, j+1, k) - 3u(i, j, k)) \quad (34)$$

$$u(i-1, j, k) = u(i+1, j, k) + \left(\frac{2\Delta z}{12\Delta x}\right) \left(\frac{\mu_{cx}}{(\mu_{cz})}\right) (-w(i, j+2, k) + 4w(i, j+1, k) - 3w(i, j, k)). \quad (35)$$

This permits the controversial horizontal point [6] of the fictitious line to be updated. With these points updated the code can compute the rest of the points of the fictitious line in the order established by a totally explicit way.

The points that are computed with this scheme are points of type [6] and [7]. In particular, those points placed nearest the exterior corners. With this scheme internal points [1] will be used to update these extreme points (see Fig. 7a).

The other way to solve this problem is to reclassify some points of the grid. In the example that occupies us it

would be necessary to transform these points as shown in Fig. 7b. The exterior corner [10] passes to be an exterior point [0]. Both extreme points [6] and [8] are converted to exterior corners [10] and an internal point of the model [1] passes to be an interior corner [2]. In this way all these points can be computed by updated points following the same order as previously indicated. This approximation can be justified because the order of magnitude of the spatial step used to discretize the model is much smaller than the dimensions of the complete grid and of the wavelengths of the waves that propagate in the model. Both ways to compute the displacements at the points [6] and [8], with forward or centered difference schemes, gave us identical results for irregular topographies. With any of these techniques and following the right order as shown here, it is possible to compute the displacement at any point of the fictitious line by a totally explicit way.

Although a method to compute the displacements at the free surface of 2D models has been presented, this scheme can also be easily extrapolated to a 3D space. To achieve this target, first it is necessary to classify the hypermatrix that will represent the model. As in the 2D case, this matrix will be full with zeros and ones, and a fictitious surface will be necessary to compute the displacements at the free surface of the model. Two basic differences exist between the 3D and 2D formulation: the expressions of stress are different,

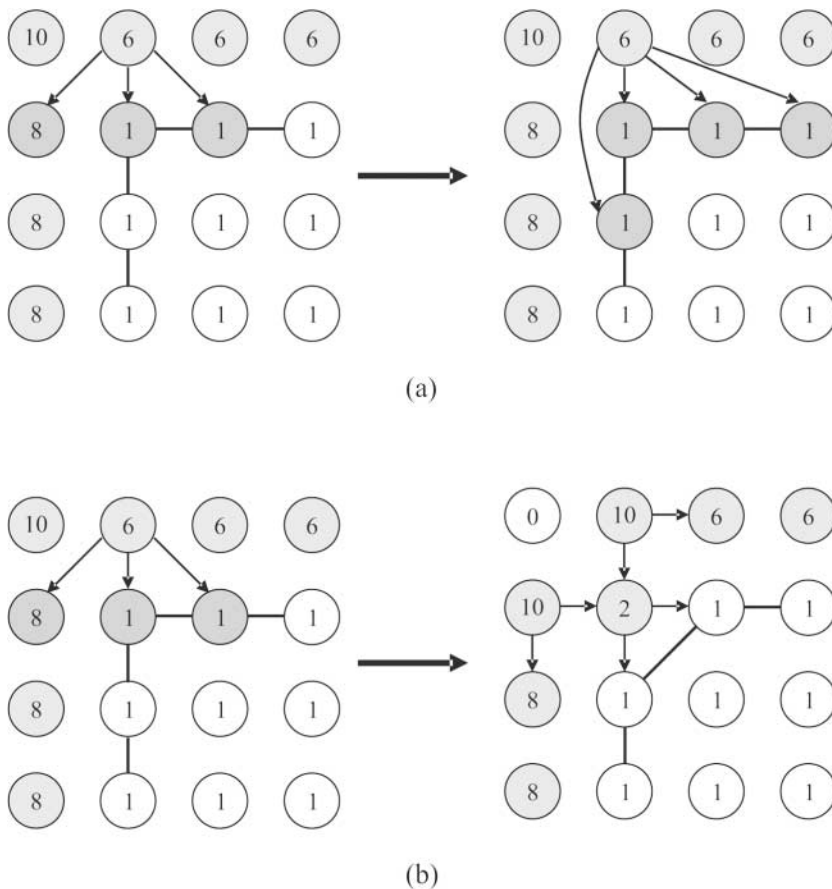


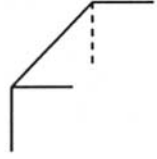
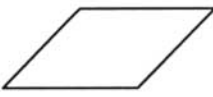
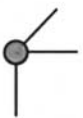

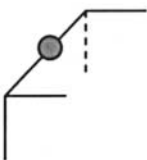
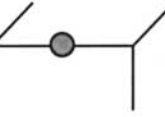
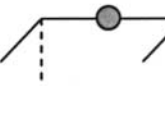



Figure 7. Two ways to solve the implicit problem at the fictitious line. (a) It is possible to change the centered FD scheme for a forward FD scheme in the conflictive point 6. (b) Reclassification of the points at the grid. Here an example is shown with the exterior corner point 10, changing some points in our classification to achieve an explicit scheme.

Table 2
Two Examples of the Procedure to Obtain the Points of the Classification of the Fictitious Surface in a 3D Model

2D (x,z)						
3D (x,y,z)						
Different points of the 3D classification						

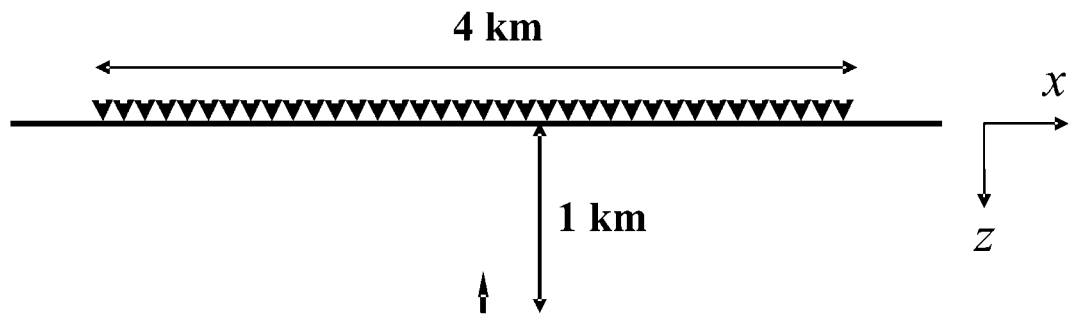


Figure 8. Half-space with planar free surface. Fifty-one receivers cover 4 km above the free surface, and they are separated by 80 m. The *P*-wave velocity is 1 km/sec and the Poisson ratio is 0.25. The source is localized to 1 km deep.

because they contain a third coordinate now, and a major number of points at the fictitious surface will be necessary categorize. In this way a whole of 46 different points are necessary.

In the 2D model there are four corners and two lineal basic elements. These elements can have material in a side or in the other one, generating a set of 12 points, that is $(4 + 2) \times 2 = 12$ (see Table 1). We can generalize from

these elements to obtain the different kinds of points in 3D. In Table 2, we present, as are example, a corner and a lineal element in 2D-(x, z), which are extended to the 3D-(x, y, z) case. It is possible observe that each 2D corner evolves to two 3D corners and one 3D edge. On the other hand, each 2D-lineal element evolves to four new 3D edges and one flat side. The rest of the 2D-elements can be treated as an analogous form. Without a lot of effort we can find, there-

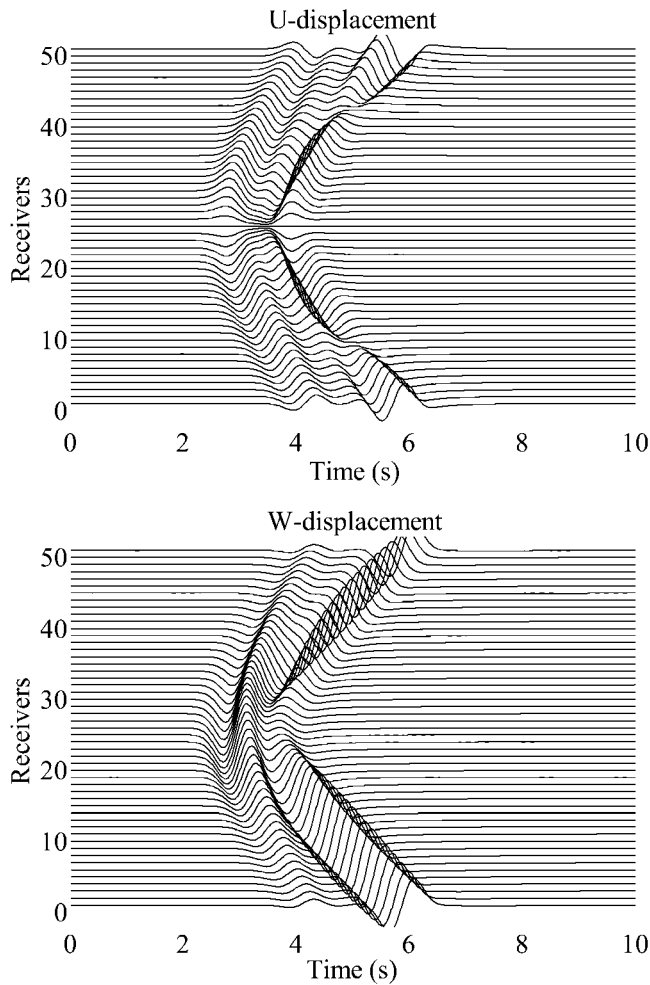


Figure 9. u and w components of the displacements at 51 receivers in the model of the homogeneous half-space produced by a vertical force. The results computed with the FD method are presented with solid lines, whereas the results from the IBEM are with dashed lines.

fore, that $(4 \times 2) \times 2 = 16$ corners, $(4 \times 1 + 2 \times 4) \times 2 = 24$ edges, and $(2 \times 1 + 1) \times 2 = 6$ flat sides can be present at the fictitious surface of a 3D model. In these computations the numbers inside the parentheses show the number of basic elements, and the multiplier 2 indicates the possibility to have material in a side or in the other one of the element. Finally each one of these elements must be treated by its corresponding stress condition.

Test Examples

To test the validity of our approach, our results are compared with those obtained using the IBEM (Sánchez-Sesma and Campillo, 1993). First, a homogeneous model with a horizontal and planar free surface is presented. This model has a P -wave velocity of 1 km/sec and a Poisson coefficient of 0.25. It was excited with a point force directed upward,

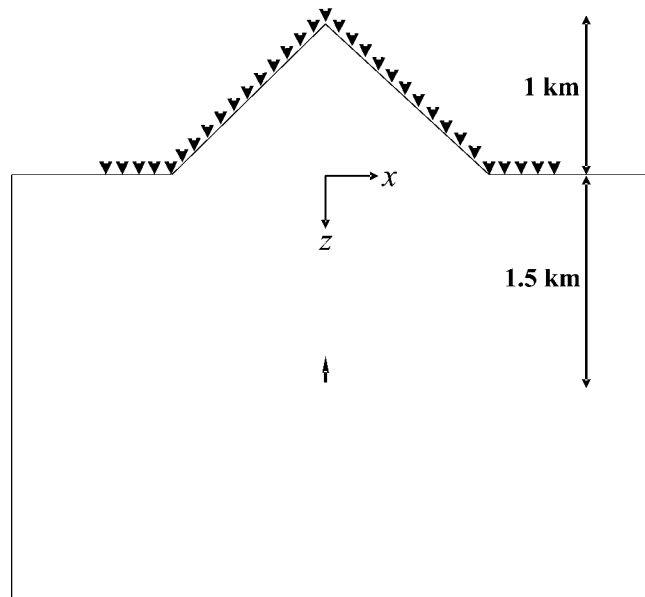


Figure 10. Model of a triangular mountain with dipping angles of 45° and a height of 1 km. In this case the half-space has a P -wave velocity of 1 km/sec and a Poisson coefficient of 0.25. The source is localized in $x = 0$ km and $z = 1.5$ km. It is an upward vertical force modeled by a Ricker wavelet with $t_p = 1$ sec and $t_s = 2$ sec. Forty-nine receivers are situated at the free surface, between $x = -1920$ m and $x = 1920$ m, and separated by a horizontal distance of 80 m.

modeled by a Ricker wavelet with $t_p = 1$ sec, and $t_s = 2$ sec. This force is located at a depth of 1 km (see Fig. 8). The vertical (w) and horizontal (u) displacements were computed at 51 receivers placed on the free surface, spaced at 80 m. The central receiver is located directly above applied force. A time step $\Delta t = 0.012$ sec and a grid spacing of $\Delta x = \Delta z = 20$ m were used. In Figure 9 the vertical (w) and horizontal (u) displacements are shown with a solid line. The solution computed using IBEM has been superposed by using a dashed line. Both solutions are in very good agreement.

Next we consider a triangular mountain centered in the origin, with dipping angles of 45° and a height of 1 km (see Fig. 10). The source considered is a vertical force embedded in the half-space and directed upward, located at $x = 0$ km and $z = 1.5$ km. The time signal is a Ricker wavelet with $t_p = 1$ sec, and $t_s = 2$ sec. The half-space has a P -wave velocity of 1 km/sec and a Poisson coefficient of 0.25. No attenuation was included. In Figure 11, horizontal (u) and vertical (w) displacement at 4 receivers located on the free surface, between $x = -1920$ m and $x = 1920$ m, and separated by 80 m are presented. This solution is calculated using a time step $\Delta t = 0.006$ sec, and a grid spacing $\Delta x = \Delta z = 10$ m. The results computed using the IBEM are shown in the same figure for comparison. Both computations are in very good agreement. In this example the P and SV waves produce creeping waves with great amplitude. Part of their energy is emitted as Rayleigh waves when they arrive at

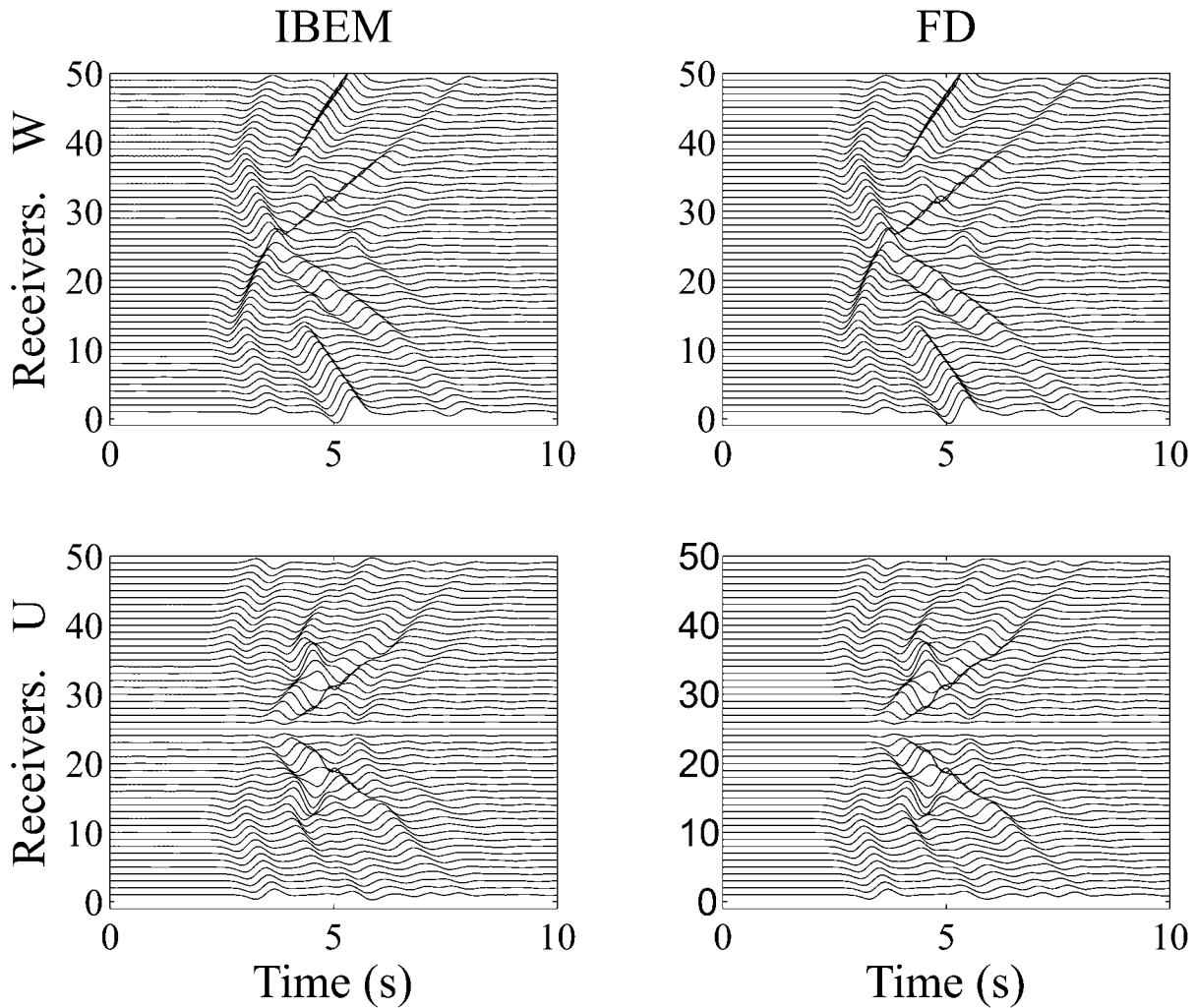


Figure 11. Synthetic seismograms recorded on the free surface of a triangular mountain, produced by a vertical force modeled by a Ricker source function. U, horizontal component; W, vertical component.

horizontal surface. Also, the P reflected from one wall to the other can be observed in the horizontal component. In Figure 12 details of the displacements at receivers 29, 38, and 44 are presented. These receivers have been chosen because they include the three different zones of the mountain. Receiver 29 is placed approximately on the middle of the right hillside of the mountain, receiver 44 is located above the half of the flat free surface, and receiver 38 is placed at the zone where the flat and hillside are joined. We can observe that numerical solution obtained by the FD method (solid line) at the three positions is in good agreement with the IBEM solution (dashed line).

As a final test, a semielliptical cavity with a major semi-axis of 1 km and a minor semi-axis of 0.5 km is studied (see Fig. 13). The properties of the half-space are the same as in the preceding case. The source is located in $x = 0$ km and $z = 2$ km, and it is modeled by a Ricker wavelet with $t_p = 1$ sec, and $t_s = 2$ sec. In this case an explosion is considered. The receivers are located on the free surface separated by a

horizontal distance of 80 m, and the same time step and grid spacing as before are used. Figure 14 presents the results together with those computed using the IBEM. The incidence of the P waves producing creeping waves as shown by Ohminato and Chouet (1997) and the appearance of Rayleigh waves that propagate at the horizontal free-surface section are observed. The displacement shows important amplifications in the vertical component at the central stations of the semielliptical canyon and in the corners.

Conclusion

In this work, we have developed a procedure to deal with an irregular free surface in a 2D FD scheme for P - SV waves. We use a regular scheme of FD in a displacement formulation. In this article the treatment of absorbing boundary conditions and a rigorous study of stability analysis and of numerical dispersion are omitted, because these topics

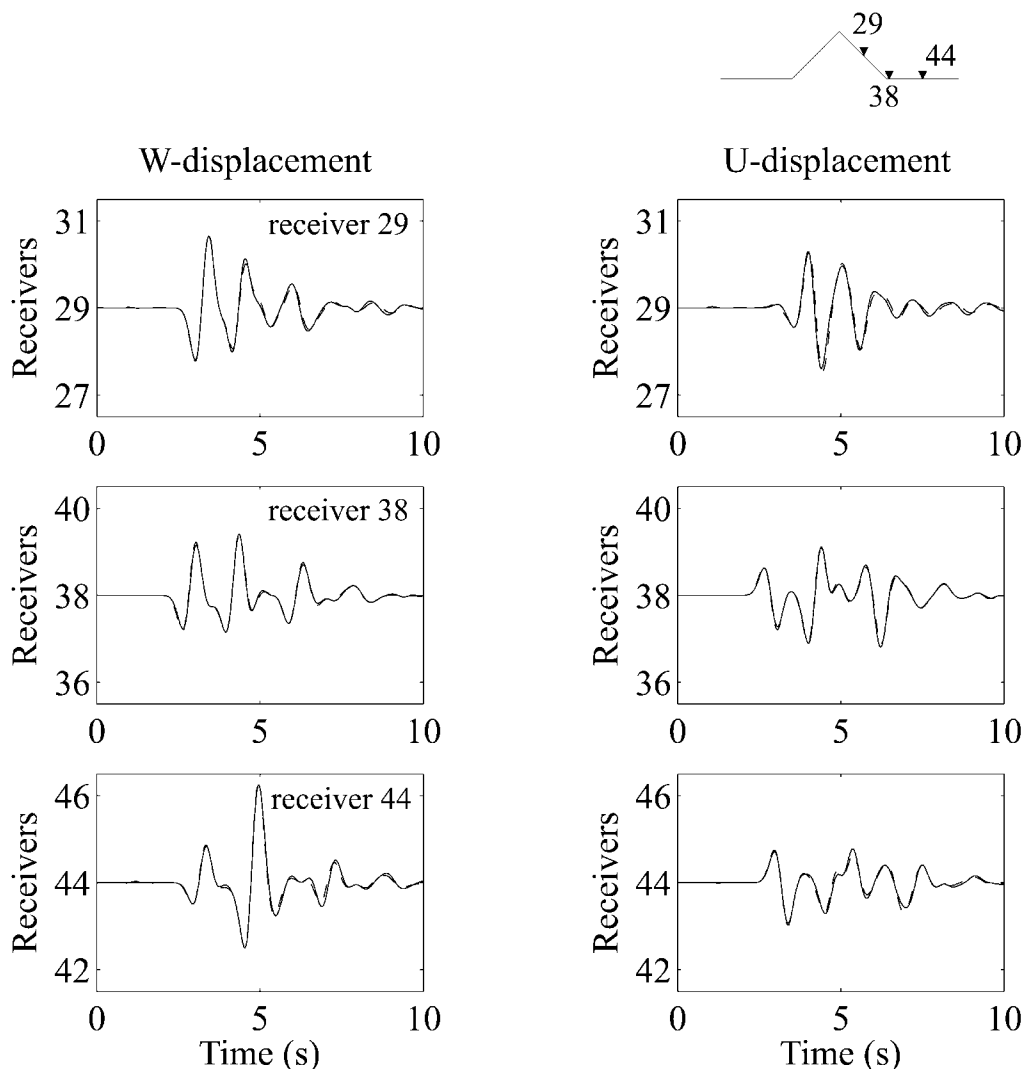


Figure 12. Detail of vertical (W) and horizontal (U) displacements in receivers 29, 38, and 44 placed above the free surface of the triangular mountain. The results obtained by the FD method (solid line) are compared with results generated by the IBEM (dashed line).

have been well described by Virieux (1986) and Levander (1988) among others.

Our procedure is based on the classification of the different points of the grid: interior points, the fictitious line points, and boundary points. This will allow computing each point with its corresponding equation in the correct order. An important aspect is the concept of a fictitious line above the free surface. Using this line, together with the cell-based grid, where the material properties are calculated by geometric averages, to compute the values of these properties in the grid cells rather than at nodal points, correct results can be obtained. The results obtained with our method have been validated with those calculated with an IBEM. Using the appropriate boundary conditions we have been able to deal with problems of seismological interest as the seismic wave propagation in a free surface with topographic features.

By using the fictitious line with the free-surface conditions and cell-based grid as developed here, the results have been satisfactory.

Acknowledgments

This work was supported in part by CICYT, Spain, under Grant REN2002-04198-C02-02/RIES, by the European Community with FEDER, the research team RNM-194 of Junta de Andalucía, Spain. We are very grateful to two anonymous referees for their constructive reviews, which significantly improved this article.

References

- Aki, K., and K. L. Larner (1970). Surface motion of a layered medium having an irregular interface due to incident plane SH waves, *J. Geophys. Res.* **75**, 933–945.

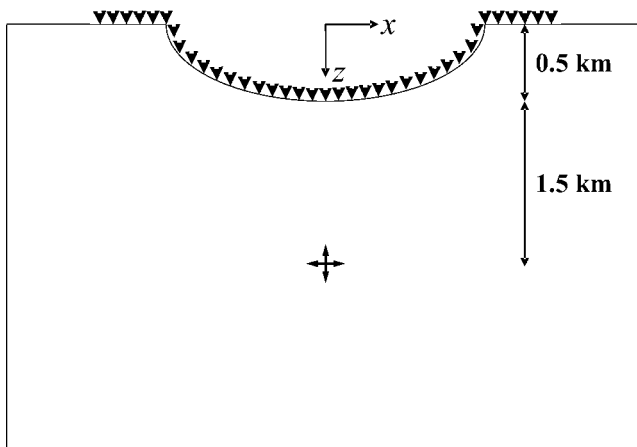


Figure 13. Model of a semielliptical canyon centred in the origin of coordinates, with a major semi-axis of 1 km and a minor semi-axis of 0.5 km, the half-space has a P -wave velocity of 1 km/sec and a Poisson coefficient of 0.25. The source is situated in $x = 0$ km and $z = 2$ km and it is modeled using a Ricker wavelet with $t_p = 1$ sec and $t_s = 2$ sec. Forty-nine receivers are situated at the free surface, between $x = -1920$ m and $x = 1920$ m, and separated by a horizontal distance of 80 m.

- Alterman, Z. S., and F. C. Karal (1968). Propagation of elastic waves in layered media by finite difference methods, *Bull. Seism. Soc. Am.* **58**, 367–398.
- Bard, P.-Y. (1994). Effects of surface geology on ground motion: recent results and remaining issues, in *Proc. of the 10th European Conference Earthquake Engineering*, Vienna, Austria, 28 August–3 September 1994.
- Bielak, J., K. Loukakis, Y. Hisoda, and Ch. Yoshima (2003). Domain reduction method for three-dimensional earthquake modelling in localized regions, part I: theory. *Bull. Seism. Soc. Am.* **93**, 817–824.
- Boore, D. M. (1972). Finite difference methods for seismic wave propagation in heterogeneous materials, in *Methods in Computational Physics*, B. A. Bolt (Editor), Vol. 11, Academic Press, New York, 1–37.
- Fuyuki, M., and Y. Matsumoto (1980). Finite difference analysis of Rayleigh wave scattering at a trench, *Bull. Seism. Soc. Am.* **70**, 2051–2069.
- Graves, R. W. (1996). Simulating seismic wave propagation in 3D elastic media using staggered-grid finite differences, *Bull. Seism. Soc. Am.* **86**, 1091–1106.
- Hayashi, K., D. R. Burns, and N. Toksöz (2001). Discontinuous-grid finite-difference seismic modeling including surface topography, *Bull. Seism. Soc. Am.* **91**, 1750–1764.
- Ilan, A. (1977). Finite difference modelling for P-pulse propagation in elastic media with arbitrary polygonal surface, *J. Geophys.* **43**, 41–58.
- Kelly, K. R., R. W. Ward, S. Treitel, and R. M. Alford (1976). Synthetic seismograms: a finite-difference approach, *Geophysics* **41**, 2–27.
- Kristek, J., P. Moczo, and R. J. Archuleta (2002). Efficient methods to simulate planar free surface in the 3D 4th order staggered-grid finite-difference schemes, *Stud. Geophys. Geod.* **46**, 355–381.
- Levander, A. R. (1988). Fourth-order finite-difference P-SV seismograms, *Geophysics* **53**, 1425–1436.
- Marfurt, K. J. (1984). Accuracy of finite-difference and finite-element modelling of the scalar and elastic wave equations, *Geophysics* **49**, 533–549.
- Min, D. J., Ch. Shin, and H. S. Yoo (2004). Free-surface boundary condition in finite-difference elastic wave modeling, *Bull. Seism. Soc. Am.* **94**, 237–250.
- Moczo, P., J. Kristek, and M. Gális (2004). Simulation of the planar surface with near-surface lateral discontinuities in the finite-difference modelling of seismic motion, *Bull. Seism. Soc. Am.* **94**, 760–768.
- Moczo, P., J. Kristek, and L. Halada (2000). 3D fourth-order staggered-grid finite-difference schemes: stability and grid dispersion, *Bull. Seism. Soc. Am.* **90**, 587–603.
- Munasinghe, M., and G. W. Farnell (1973). Finite difference analysis of Rayleigh wave scattering at vertical discontinuities, *J. Geophys. Res.* **78**, 2454–2466.
- Ohminato, T., and B. A. Chouet (1997). A free-surface boundary condition for including 3D topography in the finite-difference method, *Bull. Seism. Soc. Am.* **87**, 494–515.
- Oprsal, I., and J. Zahradník (1999). Elastic finite-difference method for irregular grids, *Geophysics* **64**, 240–250.
- Peaceman, D. W. (1966). Numerical solution of elliptic and parabolic partial differential equations, Presented at Conference on Electromagnetic Fields in Electrical Devices, National Science Foundation, Boulder, Colorado.
- Pérez-Ruiz, J. A., and F. Luzón (2004). A finite-difference method for the propagation of elastic P-SV waves, in *4^a Asamblea Hispano-Portuguesa de Geodesia y Geofísica*, (Figueira da Foz) Portugal, 293–294.
- Rong-Song, J. K. L., J. K. L. McLaughlin, and A. D. Zoltan (1988). Free-boundary conditions of arbitrary topography in a two-dimensional explicit elastic finite-difference scheme, *Geophysics* **53**, 1045–1055.
- Ruud, B., and S. Hestholm (2001). 2D surface topography boundary conditions in seismic wave modelling, *Geophys. Prospect* **49**, 445–460.
- Sánchez-Sesma, F. J. (1996). Strong ground motion and site effects, in *Computer Analysis and Design of Earthquake Resistant Structures*, D. E. Beskos and S. A. Anagnostopoulos (Editors), Computational Mechanical Publications, Southampton, 200–229.
- Sánchez-Sesma, F. J., and M. Campillo (1993). Topographic effects for incident P, SV and Rayleigh waves, *Tectonophysics* **218**, 113–125.
- Sánchez-Sesma, F. J., and F. Luzón (1995). Seismic response of three dimensional alluvial valleys for incident P, S and Rayleigh waves, *Bull. Seism. Soc. Am.* **85**, 269–284.
- Sochacki, J. S., J. H. George, R. E. Ewing, and S. B. Smithson (1991). Interface conditions for acoustic and elastic wave propagation, *Geophysics* **56**, 168–181.
- Virieux, J. (1986). P-SV wave propagation in heterogeneous media: velocity-stress finite-difference method, *Geophysics* **51**, 889–901.
- Zahradník, J., and E. Priolo (1995). Heterogeneous formulations of elastodynamic equations and finite difference schemes, *Geophys. J. Int.* **120**, 663–676.
- Zahradník, J., P. O’Leary, and J. Sochacki (1994). Finite-difference schemes for elastic waves based on the integration approach, *Geophysics* **59**, 928–937.

Department of Applied Physics
 Instituto Andaluz de Geofísica
 University of Almería
 Cañada de San Urbano s/n
 04120-Almería
 Spain

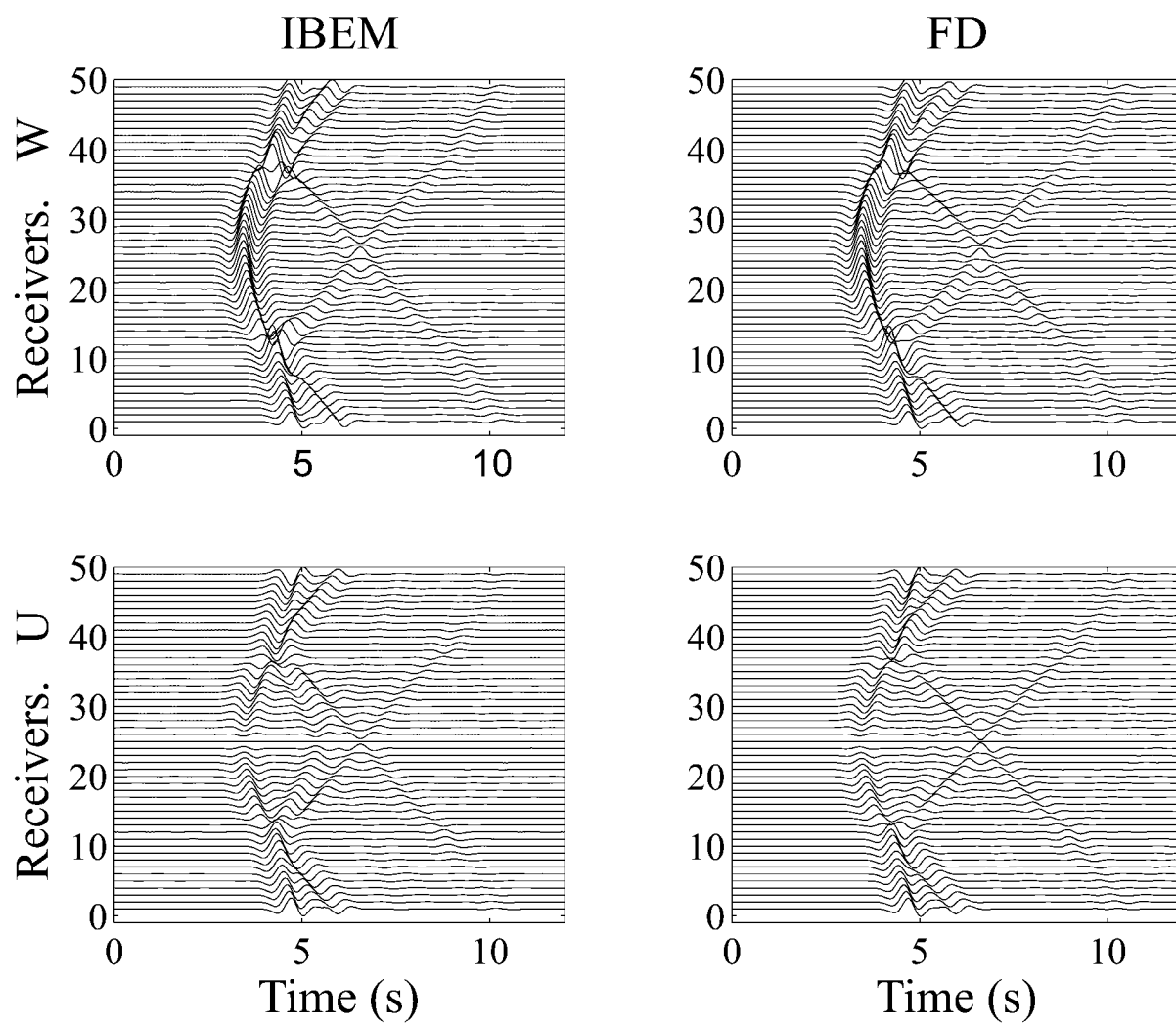


Figure 14. Synthetic seismograms recorded on the free surface of a semicircular canyon, produced by an explosive source modeled by a Ricker source function. U, horizontal component; W, vertical component.